Acta Pharmacologica Sinica

www.nature.com/aps

ARTICLE

N-n-Butyl haloperidol iodide ameliorates liver fibrosis and hepatic stellate cell activation in mice

Dai-fei Shen[1], He Cheng[2], Bo-zhi Cai[3], Wen-feng Cai[1], Bin Wang[1], Qing Zhu[1], Yue-bin Wu[1], Man Liu[1], Run-ji Chen[1], Fen-fei Gao[1], Yan-mei Zhang[1], Yong-dong Niu[1] and Gang-gang Shi[1]

N-n-Butyl haloperidol iodide (F_2) is a novel compound that has antiproliferative and antifibrogenic activities. In this study we investigated the therapeutic potential of F_2 against liver fibrosis in mice and the underlying mechanisms. Two widely used mouse models of fibrosis was established in mice by injection of either carbon tetrachloride (CCl_4) or thioacetamide (TAA). The mice received F_2 (0.75, 1.5 or 3 mg·kg^{-1}·d^{-1}, ip) for 4 weeks of fibrosis induction. We showed that F_2 administration dose-dependently ameliorated CCl_4- or TAA-induced liver fibrosis, evidenced by significant decreases in collagen deposition and c-Jun, TGF-β receptor II (TGFBR2), α-smooth muscle actin (α-SMA), and collagen I expression in the liver. In transforming growth factor beta 1 (TGF-β1)-stimulated LX-2 cells (a human hepatic stellate cell line) and primary mouse hepatic stellate cells, treatment with F_2 (0.1, 1, 10 μM) concentration-dependently inhibited the expression of α-SMA, and collagen I. In LX-2 cells, F_2 inhibited TGF-β/Smad signaling through reducing the levels of TGFBR2; pretreatment with LY2109761 (TGF-β signaling inhibitor) or SP600125 (c-Jun signaling inhibitor) markedly inhibited TGF-β1-induced induction of α-SMA and collagen I. Knockdown of c-Jun decreased TGF-β signaling genes, including TGFBR2 levels. We revealed that c-Jun was bound to the TGFBR2 promoter, whereas F_2 suppressed the binding of c-Jun to the TGFBR2 promoter to restrain TGF-β signaling and inhibit α-SMA and collagen I upregulation. In conclusion, the therapeutic benefit of F_2 against liver fibrosis results from inhibition of c-Jun expression to reduce TGFBR2 and concomitant reduction of the responsiveness of hepatic stellate cells to TGF-β1. F_2 may thus be a potentially new effective pharmacotherapy for human liver fibrosis.

Keywords: liver fibrosis; *N*-n-butyl haloperidol iodide; antifibrotic; c-Jun; TGFBR2; TGF-β signaling; human hepatic stellate cell line LX-2

Acta Pharmacologica Sinica (2022) 43:133–145; https://doi.org/10.1038/s41401-021-00630-7

INTRODUCTION

Liver fibrosis, which can progress to cirrhosis, is a major risk factor for hepatocellular carcinoma (HCC). Fibrosis is characterized by the excessive deposition of extracellular matrix (ECM) and is caused by a wound-healing response to chronic liver injury [1]. Liver fibrosis is a common pathological process in chronic viral hepatitis, nonalcoholic fatty liver disease, alcoholic liver disease, and cholestatic and autoimmune liver diseases. Hepatic stellate cells (HSCs) act as crucial fibrogenic effector cells in the progression of liver fibrosis. Quiescent HSCs are abundant in the space of Disse between hepatocytes and the sinusoidal endothelium [2]. In response to liver injury, HSCs develop a myofibroblast-like phenotype, become proliferative and contractile, synthesize ECM, and express α-smooth muscle actin (α-SMA) in a process referred to as activation [3]. Activated HSCs are the principal source of ECM in liver fibrogenesis [4]. Evidence indicates that the prevention of HSC activation could serve as a treatment for liver fibrosis.

However, fibrosis is clinically intractable. Liver fibrosis is commonly treated with drugs that target the primary disease causing the fibrosis, particularly in hepatitis B- and hepatitis C-related fibrosis. It is not clear whether these drugs are effective for the treatment of other chronic liver diseases, which currently have no treatment options. For example, there is no pharmacological therapy for nonalcoholic steatohepatitis (NASH) [5]. In advanced fibrosis, the elimination of the causative agent is not sufficient to reverse fibrogenesis. There is an urgent need for antifibrotic therapies to prevent the progression of liver fibrosis into cirrhosis, as well as to reduce the risk of developing HCC [6]. Although many compounds have been proven to be effective in vitro and in animal models, no pharmacological therapy has been validated via clinical trials and commercialized for the treatment of liver fibrosis [7]. Therefore, it is imperative to develop new drugs for the treatment of liver fibrosis.

N-n-Butyl haloperidol iodide (F_2) (Chinese national invention patent No. ZL96119098.1) is a novel compound synthesized by our group. In our previous studies, we showed that F_2 protects the myocardium from ischemic/reperfusion (I/R) or hypoxia/reoxygenation (H/R) injury by blocking L-type calcium channels [8–10]. However, in recent years, F_2 was shown to exert protective effects against myocardial injury via a calcium-independent pathway [11]. F_2 protects cardiomyocytes and

[1]Department of Pharmacology, Shantou University Medical College, Shantou 515041, China; [2]Qingyuan Maternal and Child Health Hospital, Qingyuan 511515, China and [3]Laboratory of Molecular Cardiology, The First Affiliated Hospital, Shantou University Medical College, Shantou 515041, China
Correspondence: Gang-gang Shi (ggshi@stu.edu.cn)

Received: 5 August 2020 Accepted: 17 February 2021
Published online: 23 March 2021

endothelial cells by downregulating the H/R-induced upregulation of c-Jun N-terminal kinase (JNK) phosphorylation [12, 13]. Moreover, F_2 inhibits the proliferation of vascular smooth muscle cells by reducing the expression of α-actin [14]. The aforementioned effects of F_2 could be linked to the pathological and molecular mechanisms of liver fibrosis. Our preliminary tests showed that F_2 has therapeutic potential in treating Kun-Ming mouse liver fibrosis induced by carbon tetrachloride (CCl_4). However, its antifibrotic effect needs to be further investigated, as the underlying mechanism remains unclear.

Transforming growth factor beta 1 (TGF-β1) is the most powerful stimulus for transforming quiescent HSCs into fibrogenic myofibroblasts. TGF-β1 initiates signaling by binding to TGF-β receptor II (TGFBR2); unlike the TGF-β superfamily member BMP, TGF-β must bind to TGFBR2 to transduce signals [15]. A recent study showed that TGFBR2 could transduce TGF-β signals in the absence of TGF-β receptor I (TGFBR1) [16]. Downregulating TGFBR2 expression or administering soluble TGFBR2 has been shown to ameliorate liver fibrogenesis [17, 18].

c-Jun is a component of activator protein 1 (AP-1) and heterodimerizes with other family members, such as Jun, Fos and ATF, to form AP-1 transcription factors [19]. AP-1 controls multiple cellular physiological and pathological processes and recognizes 12-O-tetradecanoylphorbol-13-acetate response elements. c-Jun has a high binding affinity and is the most positive transcriptional activator in this group. Previous studies have shown that c-Jun expression is enhanced in fibrotic livers [20]. Inhibiting AP-1 activity suppresses HSC activation [21]. In HBV^+ mice, c-Jun is strongly expressed during tumorigenesis, while the expression of other AP-1 members remains unchanged [22]. Increasing hepatic c-Jun levels promotes NASH progression [23]. c-Jun is an archetypical target of JNK. JNK is involved in the activation of HSCs and the progression of liver fibrosis [24]. The phosphorylation of JNK and its target c-Jun is strongly increased in mouse livers following bile duct ligation or CCl_4 administration, as well as in human fibrotic livers, and this phosphorylation predominantly occurs in myofibroblasts. Inhibiting JNK phosphorylation therefore prevents liver fibrosis [25].

In this study, we investigated the antifibrotic effect of F_2 on a hepatic stellate cell line activated by recombinant TGF-β1 and primary mouse HSCs, as well as on two widely used animal models of liver fibrosis: CCl_4-induced and thioacetamide (TAA)-induced fibrosis in C57BL/6J mice. We aimed to determine whether F_2 was a potential therapeutic agent to ameliorate liver fibrosis and whether its mechanism could be attributed to the reduced responsiveness of HSCs to TGF-β1.

MATERIALS AND METHODS

Animals

All animal experiments were approved by the Institutional Animal Care and Use Committee of Shantou University Medical College (Approval No: SUMC2019165).

Male C57BL/6J mice were purchased from Vital River Company (Beijing, China) and were maintained and bred in the SPF animal facility of Shantou University Medical College under a 12 h light/12 h dark cycle with standard temperature and humidity and free access to mouse chow and water. The animals were acclimatized for 7 days before experimentation.

Reagents

F_2 was synthesized by our group, and the chemical structure can be found in the reference [10]. CCl_4, olive oil, and TAA were purchased from Aladdin Chemistry Co., Ltd. (Shanghai, China) and Sigma-Aldrich (St Louis, MO, USA), respectively. Recombinant human TGF-β1 (#100-21 C) was obtained from PeproTech (Rocky Hill, NJ, USA). LY2109761 (HY-12075) was obtained from MCE (Shanghai, China), and SP600125 (S1460) was obtained from Selleck Chemicals (Houston, TX, USA). Anti-p-Smad2/3 (#8828), anti-Smad2/3 (#8685), anti-c-Jun (#9165), and anti-p-c-Jun (#3270) were obtained from Cell Signaling Technology (Danvers, MA, USA). Anti-α-SMA (A5228), anti-collagen I (ab34710), and anti-TGFBR2 (66636-1-Ig) were purchased from Sigma-Aldrich (St Louis, MO, USA), Abcam (Cambridge, UK), and Proteintech (Wuhan, China), respectively. Anti-GAPDH (TA-08) and anti-β-actin (TA-09) were obtained from ZSGB-BIO (Beijing, China).

For in vitro experiments, F_2, LY2109761, and SP600125 were dissolved in dimethyl sulfoxide (DMSO, Amresco, Boise, ID, USA) and further diluted to the required concentrations (the final DMSO concentration in the solution was ≤0.1%). For in vivo experiments, F_2 was dissolved in a saline solution containing 0.5% DMSO and 0.75% Tween 20 (Amresco, Boise, ID, USA). This solvent had no effect on collagen deposition, as shown in Supplementary Fig. S1.

Mouse liver fibrosis model

Eight-week-old male C57BL/6J mice were injected twice per week with 1:3 CCl_4 in olive oil or olive oil alone (vehicle control mice) by intraperitoneal (ip) injection (2 mL/kg body weight) for 4 weeks. The mice were randomly divided into 6 groups ($n = 8$ for each group): vehicle control group, F_2 (3 mg/kg, ip) plus olive oil control group, CCl_4 group, and CCl_4 plus different doses of F_2 (0.75 or 1.5 or 3 mg/kg, ip) groups. The mice received a daily injection of either F_2 or solvent beginning at the time of the first injection to induce liver fibrosis until the end of the experiment. The dose of F_2 was determined according to our preliminary tests. The mice were euthanized 48 h after the last CCl_4 injection.

Eight-week-old male C57BL/6J mice were injected three times per week with 100 mg/kg TAA dissolved in saline (10 mL/kg, 1% *w/v*) or saline alone (vehicle control mice) by ip injection for 8 weeks. The mice were randomly divided into 6 groups ($n = 8$ for each group): vehicle control group, F_2 (3 mg/kg, ip) plus saline control group, TAA group, and TAA plus different doses of F_2 (0.75 or 1.5 or 3 mg/kg, ip) groups. Four weeks after the TAA injection, F_2 treatment was initiated, and the mice received a daily injection of either F_2 or solvent for the final 4 weeks of fibrosis induction. The dose of F_2 was determined according to our preliminary tests. The mice were euthanized 72 h after the last TAA injection.

The animals were anesthetized with sodium pentobarbital (1%) by ip injection, blood samples were collected, the mice were euthanized via CO_2 administration, and liver samples were isolated and divided into 3 parts. One part of the liver was fixed in 4% paraformaldehyde in PBS and prepared for histological analyses, and another part was used to prepare homogenates. The remaining liver tissues were snap frozen and cryopreserved at −80 °C. After clotting at room temperature, serum was separated and divided into 3 aliquots and stored at −80 °C until use.

Liver enzymes, hyaluronic acid, and hydroxyproline

Serum levels of alanine transaminase (ALT) and aspartate transaminase (AST) were measured by an automatic chemistry analyzer (Toshiba Medical Systems Corporation, Tokyo, Japan). The levels of serum hyaluronic acid and hepatic hydroxyproline were measured by using a colorimetric assay kit (Nanjing Jiancheng Biotechnology Institute Co., Ltd, Nanjing, China) according to the manufacturers' instructions.

Enzyme-linked immunosorbent assay (ELISA)

The expression of TGF-β1 was measured in serum using commercial mouse ELISA kits (4A Biotech, Beijing, China) based on a standard sandwich ELISA protocol.

Liver sections

Paraffin-embedded mouse livers were cut into 4 mm-thick sections. The sections were stained with Sirius red and Masson's trichrome (Leagene Biotechnology Co., Ltd, Beijing, China) to

evaluate liver fibrosis. For immunohistochemistry, the liver sections were deparaffinized and rehydrated, treated with 3% H_2O_2 for 20 min, blocked with goat serum (Boster Biological Technology Co., Ltd, Wuhan, China) for 40 min, and then labeled with antibodies against α-SMA (1:800) and TGFBR2 (1:600) overnight. The sections were incubated with a biotinylated secondary antibody and then stained with an avidin–biotin peroxidase complex kit (Gene Tech Co., Ltd, Shanghai, China). The stained sections were counterstained with hematoxylin for 8 min, and then images were captured with an Olympus microscope (Olympus, Tokyo, Japan).

Cell culture

The immortalized human hepatic stellate cell line LX-2 was obtained from the Cell Bank of Tongpai Biotechnology Co., Ltd. (Shanghai, China). LX-2 cells were cultured in Dulbecco's modified Eagle's medium (DMEM, Gibco, Grand Island, NY, USA) containing 2% fetal bovine serum (Gibco, Grand Island, NY, USA), 100 mg/mL streptomycin and 100 U/mL penicillin (Beyotime Institute of Biotechnology, Shanghai, China). The cells were incubated at 37 °C in a humidified atmosphere with 95% air and 5% CO_2. The cells were cultured for 24 h, and then the medium was changed to serum-free DMEM supplemented with 0.2% bovine serum albumin (BSA, Sigma-Aldrich, St Louis, MO, USA) for 24 h prior to various assays. Subsequently, recombinant human TGF-β1 was added to the cells and incubated for 24 h. F_2 was added at the same time as the addition of TGF-β1. For pathway inhibition, the cells were pretreated with LY2109761 (2.5 μM) and SP600125 (10 μM) for 30 min and 1 h, respectively, before the addition of TGF-β1. The detailed cell transfection assay is described below.

Primary HSC isolation and culture

Primary mouse HSCs were isolated according to a modified version of a previously reported protocol [26]. In brief, the liver underwent two-step perfusion in situ through the hepatic portal vein. Percoll (40%, Pharmacia, GE Healthcare, Pittsburgh, PA, USA) was prepared by diluting 100% Percoll with a cell suspension and overlaid with 25% Percoll to form a discontinuous Percoll density gradient. The isolated HSCs were cultured in DMEM with 20% FBS and 1% antibiotics at 37 °C in a humidified atmosphere with 95% air and 5% CO_2. After 48 h, the medium was replaced with DMEM containing 10% FBS, and the cells were continuously cultured. Different concentrations of F_2 were added and incubated for 3 days (the medium was changed once per day) beginning on the fifth day after isolation, and the treatment time was determined by the results of preliminary experiments.

Protein sample preparation and Western blotting

Liver tissues and cells were lysed in radioimmune precipitation assay (RIPA) buffer containing a protease and phosphatase inhibitor cocktail (Beyotime Institute of Biotechnology, Shanghai, China). Total protein concentrations were quantified with a BCA assay kit (Thermo Fisher Scientific Inc., Rockford, IL, USA). Equal quantities of protein were separated by 8%–12% SDS-PAGE and transferred onto nitrocellulose membranes, which were then blocked with 5% skimmed milk and probed at 4 °C overnight with primary antibodies against α-SMA (1:2000), collagen I (1:4000), p-Smad2/3 (1:1500), Smad2/3 (1:1000), TGFBR2 (1:2000), c-Jun (1:2000), p-c-Jun (1:1000), GAPDH (1:2000), and β-actin (1:2000). GAPDH and β-actin were used as loading controls. After the membranes were washed, HRP-conjugated goat anti-mouse/rabbit secondary antibodies (ZSGB-BIO, Beijing, China) were added and incubated for 2 h at room temperature, and signals were detected by a SuperSignal detection kit (Thermo Fisher Scientific Inc., Rockford, IL, USA).

Total RNA preparation and real-time polymerase chain reaction (RT-PCR)

Total RNA was extracted from liver tissues and LX-2 cells with TRIzol reagent (Takara Bio Inc., Dalian, China) according to the manufacturer's protocol. cDNA was obtained by reverse transcription using a Takara reverse transcription kit (Takara Bio Inc., Dalian, China). RT-PCR analysis was performed with SYBR Green I dye on an ABI Prism 7500 sequence detection system (Applied Biosystems, Foster City, CA, USA) according to the manufacturer's protocol. The primers used are listed in the Supplementary Table S1. GAPDH and β-actin were used as quality controls. Relative target mRNA expression was evaluated by the $2^{-\Delta\Delta Ct}$ method.

Immunofluorescence staining

LX-2 cells were seeded onto 1.2 cm^2 cover slips. After treatment, the cells were fixed in 4% paraformaldehyde in PBS for 15 min at room temperature and permeabilized in 0.1% Triton X-100 PBS for 10 min. BSA (2%) was added and incubated for 1 h to block nonspecific binding sites, and then the cells were incubated with primary antibodies against α-SMA (1:800), c-Jun (1:400), and TGFBR2 (1:200) overnight at 4 °C, followed by incubation with a fluorescein-conjugated secondary antibody (Invitrogen Life Technologies, Carlsbad, CA, USA) for 1 h. Nuclei were stained with DAPI (Beyotime Institute of Biotechnology, Shanghai, China) for 15 min. The stained cells were visualized using an Olympus microscope (Olympus, Tokyo, Japan).

Small interfering RNA (siRNA) and plasmid transfection

LX-2 cells were seeded in six-well plates and incubated for no more than 24 h to confirm the transfection efficiency. Cells were transfected with siRNA or plasmids using Lipofectamine 2000 reagent (Invitrogen, Carlsbad, CA, USA) in serum-free medium (Gibco, Grand Island, NY, USA) according to the manufacturers' instructions. Human c-Jun siRNA (sc-29223) was a commercial siRNA obtained from Santa Cruz Biotechnology (Santa Cruz, CA, USA). Human TGFBR2 siRNA and negative control siRNA were obtained from Biotend Co., Ltd. (Shanghai, China), and the target sequences are listed in the Supplementary Table S2. The TGFBR2 overexpression plasmid (pCMV-TGFBR2) and negative control plasmid (pCMV-control) were constructed by Jikai Genochemical Technology Co., Ltd. (Shanghai, China). Twenty-four hours after transfection, the cells were subsequently treated with 5 ng/mL TGF-β1 for an additional 24 h and harvested to measure the expression of the target genes.

Chromatin immunoprecipitation (ChIP)

After LX-2 cells were treated with TGF-β1 or TGF-β1 plus F_2 (or vehicle control), the cells were collected, crosslinked with formaldehyde, lysed and sonicated to generate DNA fragments. The lysates were incubated with anti-c-Jun antibodies overnight at 4 °C and then bound to protein G agarose beads. The immunoprecipitated chromatin was then eluted and purified using a ChIP kit (Cell Signaling Technology, Danvers, MA, USA) according to the manufacturer's instructions. Immunoprecipitated DNA and input control DNA were subjected to RT-PCR using SYBR Green and PCR electrophoresis on a 1% agarose gel. The primer sequences are listed in the Supplementary Table S3.

Statistical analyses

All values are expressed as the mean ± SD. Statistical analysis was performed using an unpaired Student's *t* test or Wilcoxon rank-sum test where appropriate. One-way ANOVA with the Bonferroni post hoc test was used if the data achieved normality and homogeneity of variance. P values <0.05 were considered statistically significant.

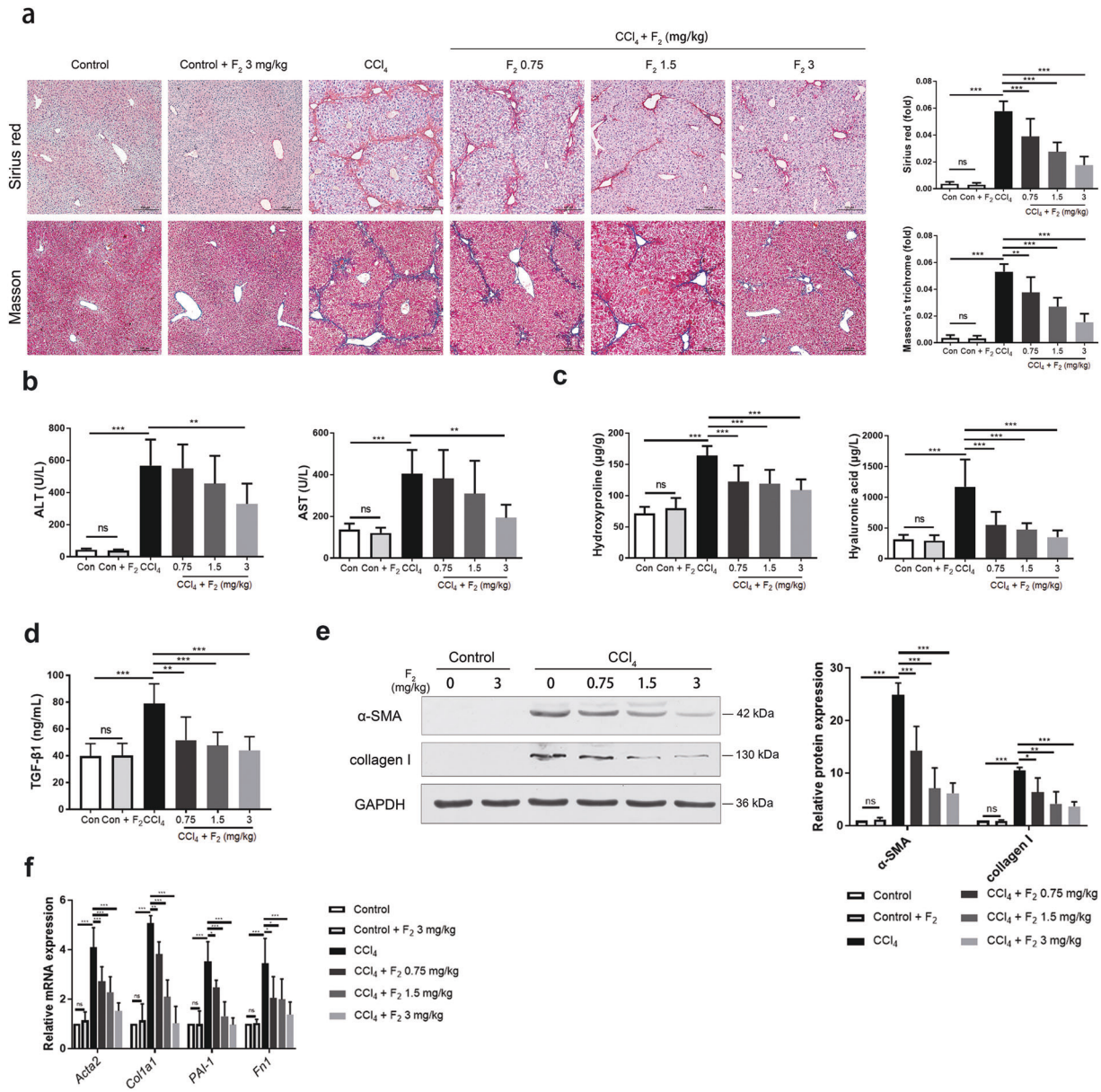

Fig. 1 F_2 treatment inhibits CCl_4-induced liver fibrosis in mice. a Representative stained sections of mouse livers after CCl_4 administration for 4 weeks, with or without F_2 treatment, and quantification of the stained areas. Collagen deposition was determined by Sirius red (scale bar, 100 μm) and Masson's trichrome (scale bar, 100 μm) staining. **b** Serum levels of ALT and AST. **c** Serum levels of hyaluronic acid and hepatic levels of hydroxyproline (a marker of fibrosis) were measured by a colorimetric assay kit. **d** Serum levels of TGF-β1 were measured by ELISA. **e** Protein expression levels of α-SMA and collagen I in mouse liver samples were analyzed by Western blotting. **f** The mRNA levels of *Acta2*, *Col1a1*, *PAI-1*, and *Fn1* were analyzed by RT-PCR. The values are the mean ± SD; $^*P < 0.05$; $^{**}P < 0.01$; $^{***}P < 0.001$, ns not significant, $n = 8$ mice per group.

RESULTS

F_2 ameliorates CCl_4-induced liver fibrosis in mice

To evaluate the effect of F_2 on liver fibrosis in vivo, the classic CCl_4-induced liver fibrosis animal model was used. As shown in Fig. 1a, liver sections were histopathologically assessed to determine the therapeutic effect of F_2 on liver fibrosis. Severe septal liver fibrosis was clearly observed in the CCl_4-treated group based on Masson's trichrome and Sirius red staining. Hepatic architecture was disrupted, collagen content was increased, and bridging fibrosis was established compared with those in the control group. F_2 treatment reduced the extent of collagen deposition in a dose-dependent manner, especially in the high-dose F_2 group, which exhibited only mild collagen deposition without the development of bridging fibrosis. In addition, CCl_4 increased serum levels of ALT and AST, which are predictive of liver cell damage. ALT and AST levels were significantly lower in the 3 mg/kg F_2-treated group than in the CCl_4 group. Low doses of F_2 (0.75 and 1.5 mg/kg) partially rescued hepatic function but did not significantly reduce ALT levels compared with those in the control group (Fig. 1b). The antifibrotic effect of F_2 was assessed by biochemical analysis of serum hyaluronic acid and liver hydroxyproline. We found that the increases in hydroxyproline and hyaluronic acid levels induced by CCl_4 were completely prevented by F_2 in a dose-dependent manner (Fig. 1c). In addition, ELISA revealed that F_2 reduced serum levels of TGF-β1 (Fig. 1d). Moreover, F_2 reduced the levels of α-SMA and collagen I in a dose-dependent manner, as assessed by

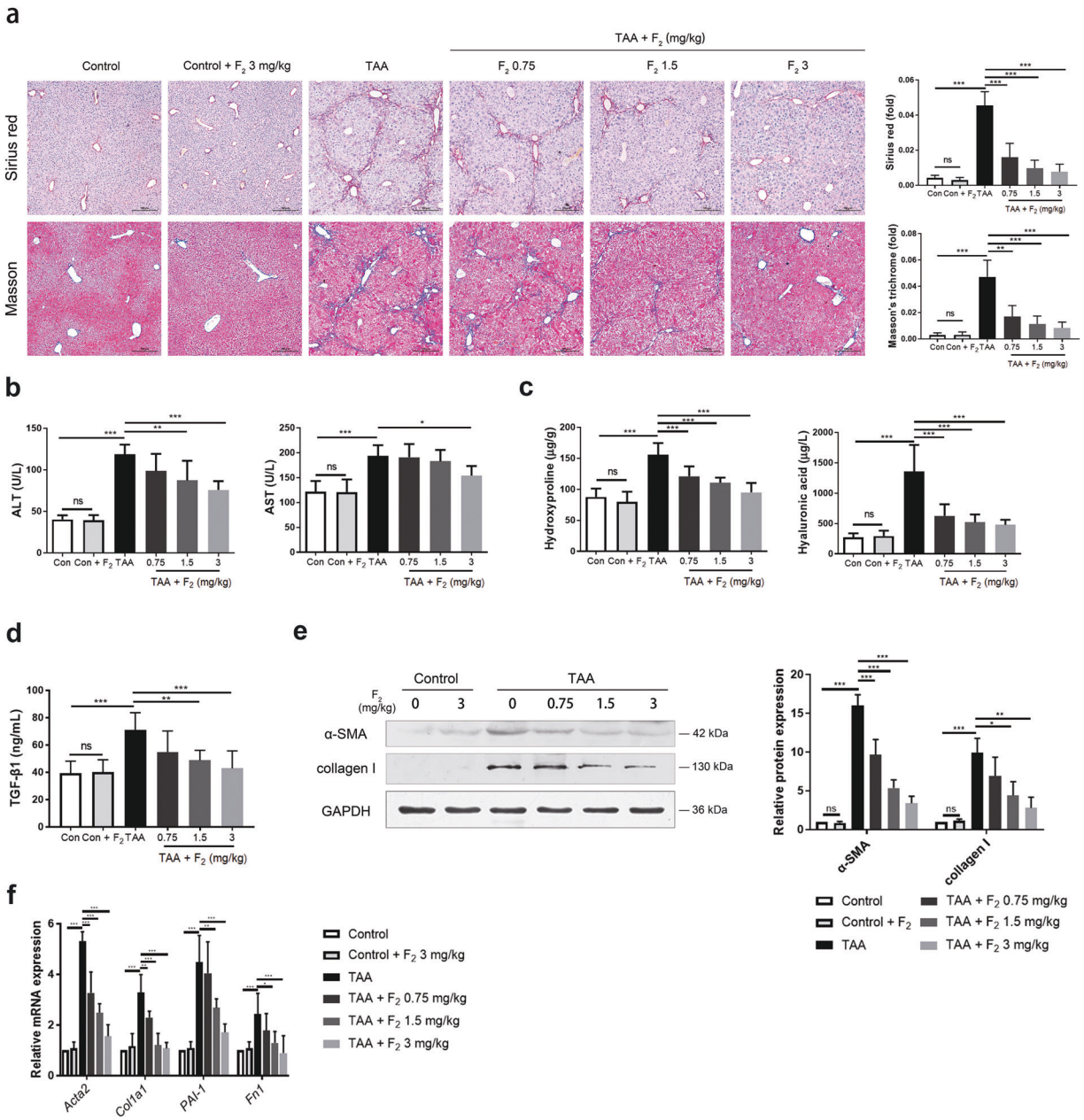

Fig. 2 F_2 alleviates TAA-induced liver fibrosis in mice. **a** Representative stained sections of mouse livers after TAA administration for 8 weeks, with or without F_2 treatment, and quantification of the stained areas. Collagen deposition was determined by Sirius red (scale bar, 100 μm) and Masson's trichrome (scale bar, 100 μm) staining. **b** Serum levels of ALT and AST. **c** Serum levels of hyaluronic acid and hepatic levels of hydroxyproline (as a marker for fibrosis) were measured by a colorimetric assay kit. **d** Serum levels of TGF-β1 were measured by ELISA. **e** Protein expression levels of α-SMA and collagen I in mouse liver samples were analyzed by Western blotting. **f** The mRNA levels of *Acta2*, *Col1a1*, *PAI-1*, and *Fn1* were analyzed by RT-PCR. The values are the mean ± SD; $^*P < 0.05$; $^{**}P < 0.01$; $^{***}P < 0.001$, ns not significant, $n = 8$ mice per group.

Western blotting (Fig. 1e). The effects of F_2 on CCl_4-induced liver fibrosis were further assessed by measuring the mRNA levels of α-smooth muscle actin (*Acta2*), *Col1a1*, Fibronectin (*Fn1*), and *PAI-1* (Fig. 1f).

F_2 alleviates TAA-induced liver fibrosis in mice

To further assess the therapeutic effect of F_2 on liver fibrosis, another widely used experimental model was used: the TAA-induced fibrosis model. Using this model, we observed portal–portal and portal–central fibrosis and biliary ductular proliferation. F_2 reduced collagen deposition and fibrous areas, as observed by Sirius red staining and Masson's trichrome staining (Fig. 2a). The histology corresponded to the reduced levels of hepatic hydroxyproline and serum hyaluronic acid observed after F_2 treatment (Fig. 2c). Serum ALT was significantly increased in the TAA-treated group compared to the control group, and this increase was significantly prevented by F_2. The TAA-mediated increase in serum AST was significantly reduced by 3 mg/kg F_2, but lower F_2 doses showed no significant effects on serum AST levels (Fig. 2b). In addition, F_2 decreased the secretion of TGF-β1 in the TAA-induced model (Fig. 2d). Similar to those in the CCl_4 model, the protein levels of α-SMA and collagen I, as well as the mRNA levels of *Fn1* and *PAI-1*,

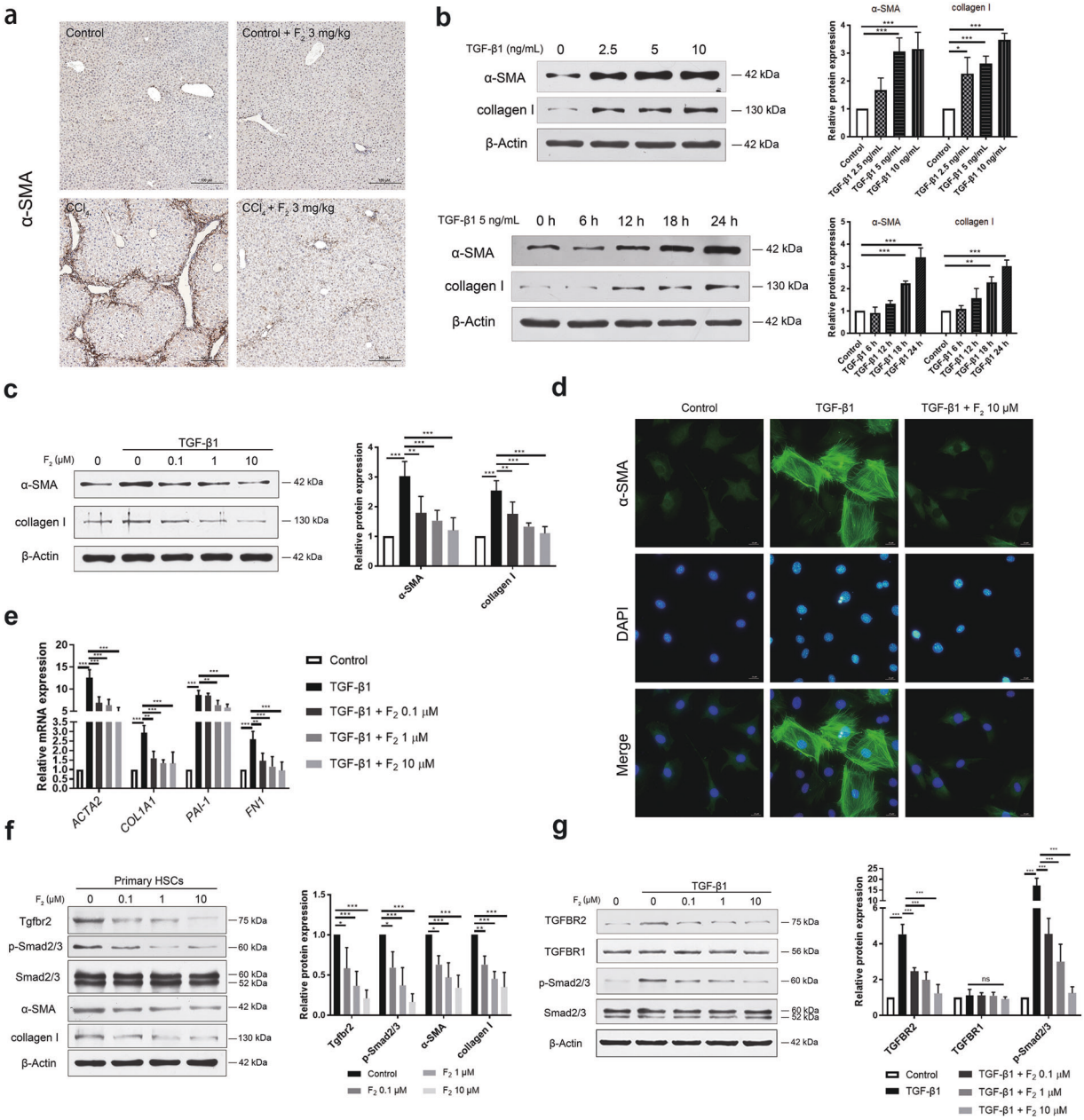

Fig. 3 F_2 inhibits TGF-β1-induced activation of hepatic stellate cells. **a** Representative images of immunohistochemical staining of α-SMA (scale bar, 100 μm). **b** Concentration-dependent and time-dependent increases in α-SMA and collagen I protein expression were stimulated by the indicated concentrations of TGF-β1. **c** Protein expression of α-SMA and collagen I was analyzed by Western blotting. **d** Immunofluorescence staining of α-SMA (green, scale bar, 20 μm) in LX-2 cells induced by 5 ng/mL TGF-β1 for 24 h with or without the indicated concentrations of F_2. **e** The mRNA levels of *ACTA2*, *COL1A1*, *PAI-1*, and *FN1* were analyzed by RT-PCR. **f** Protein expression levels of Tgfbr2, p-Smad2/3, α-SMA, and collagen I in primary mouse HSCs. **g** Western blotting analysis of TGFBR2, TGFBR1, and p-Smad2/3 protein expression in LX-2 cells treated with 5 ng/mL TGF-β1 for 24 h with or without the indicated concentrations of F_2. The values are the mean ± SD; $^*P < 0.05$; $^{**}P < 0.01$; $^{***}P < 0.001$, ns not significant, $n = 4$ cells per group.

decreased following F_2 treatment compared with those in the TAA-treated group (Fig. 2e, f).

F_2 suppresses the activation of HSCs by inhibiting TGF-β signaling To uncover the mechanism underlying the antifibrotic effect of F_2, we investigated whether F_2 regulated the expression of fibrogenic genes and the accumulation of myofibroblasts. Immunohistochemical analysis showed the accumulation of α-SMA, a myofibroblast marker, in septal liver fibrosis, along with the disruption of hepatic architecture. F_2 treatment caused a reduction in the α-SMA-positive area (Fig. 3a). Activated HSCs participate in liver fibrogenesis, serving as a source of myofibroblasts. After serum deprivation and recombinant TGF-β1 stimulation, LX-2 cells (a human HSC line) exhibited increased responsiveness to stimuli, resulting in the development of an active phenotype. We evaluated the effect of F_2 on these cells in vitro. Treatment of LX-2 cells with TGF-β1 led to a significant increase in α-SMA, indicating cellular activation. The expression of collagen I also increased in a concentration-dependent manner (Fig. 3b). F_2 significantly reduced the upregulation of α-SMA and collagen I

(Fig. 3c). Immunofluorescence staining showed strong induction of α-SMA-positive staining (green) by TGF-β1, which was largely inhibited by F_2 (Fig. 3d). The mRNA levels of *ACTA2*, *COL1A1*, *PAI-1*, and *FN1* were also decreased by F_2 (Fig. 3e). Moreover, we observed a similar antifibrotic effect of F_2 on primary mouse HSCs. As primary HSCs were subjected to spontaneous activation in culture, α-SMA staining was positive at 7 days after isolation (Supplementary Fig. S2a). Treatment with F_2 inhibited the expression of α-SMA, collagen I, Tgfbr2 and p-Smad2/3 in a dose-dependent manner (Fig. 3f). In addition, F_2 decreased the secretion of TGF-β1 in the supernatant of primary HSCs (Supplementary Fig. S2b).

These results demonstrate that F_2 exerts an inhibitory effect on TGF-β1-induced upregulation of fibrogenic markers. We ascertained whether F_2 prevented HSC activation by intervening in the canonical fibrogenic TGF-β signaling pathway. We found that F_2 blocked the upregulation of p-Smad2/3. Moreover, TGF-β-mediated expression of TGFBR2 was reduced by F_2, whereas TGFBRI expression was unchanged by TGF-β1 or F_2 (Fig. 3g). We also performed time-course experiments to examine the effects of F_2 on the phosphorylation of Smad2/3, TGFBR2, and c-Jun. We observed that F_2 downregulated the protein levels of TGFBR2 and c-Jun earlier than it downregulated those of p-Smad2/3 (Fig. 4a). These results suggest that F_2 inhibited TGF-β/Smad signaling by altering the levels of TGFBR2.

The inhibitory effect on Tgfbr2 was assessed in CCl_4- and TAA-induced mouse fibrosis models (Fig. 4c). Immunohistochemical analysis showed that Tgfbr2 was weakly expressed throughout the hepatic parenchyma and was strongly expressed in the periportal areas in CCl_4-induced fibrosis, which coincided histologically with the α-SMA-positive areas. F_2 markedly reduced the number of accumulated α-SMA-positive cells (Fig. 4b).

F_2 targets c-Jun to inhibit TGF-β signaling in HSCs

A recent study reported that c-Jun is highly expressed during various stages of liver diseases [27]. Similar results were observed in our study: c-Jun was more highly expressed in CCl_4- and TAA-treated mice than in untreated mice. F_2 reduced the expression of c-Jun (Fig. 4d). The levels of c-Jun and p-c-Jun were reduced following F_2 treatment in TGF-β1-activated LX-2 cells (activated HSCs) (Fig. 4e).

To determine the pathway underlying the inhibition of TGF-β signaling, c-Jun and TGFBR2 expression was inhibited. The protein kinase inhibitors LY2109761 and SP600125 were used to inhibit TGF-β signaling and the c-Jun pathway, respectively. Pretreatment with LY2109761 inhibited TGF-β signaling and reduced TGF-β1-mediated induction of α-SMA and collagen I (Fig. 5b). Inhibition of c-Jun with SP600125 decreased the expression of c-Jun, p-c-Jun, and TGF-β signaling genes (Fig. 5c). Similar results were obtained by immunofluorescence analysis. LY2109761 and SP600125 reduced α-SMA expression and inhibited the activated phenotype following treatment with TGF-β1 (Fig. 5a).

To confirm this finding, we transfected cells with siRNA and plasmids. Knockdown of TGFBR2 decreased the levels of p-Smad2/3, α-SMA, and collagen I (Fig. 6a). After TGF-β1 stimulation, the levels of p-Smad2/3, α-SMA, and collagen I were higher than those in vector-transfected cells, and the antifibrotic effect of F_2 was reduced by TGFBR2 expression (Fig. 6b).

F_2 decreases the binding of c-Jun to the TGFBR2 promoter

Immunofluorescence staining showed that c-Jun was mainly located in the nucleus, while TGFBR2 was expressed in both the nucleus and cytoplasm (Fig. 7a). siRNA-mediated c-Jun knockdown impaired TGF-β signaling and TGFBR2 expression (Fig. 7b), indicating a relationship between c-Jun and TGFBR2. c-Jun overexpression increased the levels of α-SMA and collagen I, while the antifibrotic effect of F_2 was counteracted by c-Jun expression (Supplementary Fig. S3). These results indicate that the mechanism by which F_2 mediates the reduction in fibrogenic genes may be associated with the inhibition of c-Jun, thus reducing TGFBR2 expression and disrupting TGF-β-mediated responses. Moreover, the level of *TGFBR2* mRNA was significantly decreased in F_2-treated cells, suggesting that F_2 can control the TGF-β pathway by inhibiting TGFBR2 transcription. The same finding was observed in c-Jun siRNA-transfected cells (Fig. 7c). To examine the resulting modulation of TGFBR2 expression, we hypothesized that F_2 modulates c-Jun binding to the TGFBR2 promoter and downregulates the transcription of TGFBR2. We then analyzed the promoters using the JASPAR and PROMO databases to predict specific transcription factor binding sites and compared these sites with the relevant references [28, 29]. The −219/+35 sequence was chosen for ChIP-qPCR primers to probe regions of the TGFBR2 promoter. ChIP-qPCR analysis of LX-2 cells after the addition of TGF-β1 revealed that c-Jun was increasingly bound to the TGFBR2 promoter. In addition, F_2 decreased the binding of c-Jun to the TGFBR2 promoter (Fig. 7d). A representative gel image of the ChIP samples is shown in Supplementary Fig. S4.

DISCUSSION

Liver fibrosis is a risk factor for cirrhosis, which can progress to HCC if poorly controlled. To avoid these life-threatening complications, antifibrotic pharmacotherapies must be developed. In this study, we investigated the therapeutic effect of F_2 on liver fibrosis in two widely used animal models. CCl_4 causes a chain reaction of lipid peroxidation and subsequent cell damage [30], and reactive TAA metabolites bind covalently to proteins and lipids, causing damage [31]. Histopathological examination showed that CCl_4 administration resulted in fatty changes in hepatocytes, with uniform bridging fibrosis [32], while TAA led to increased periportal infiltration and ductal proliferation. Both CCl_4 and TAA-induced centrilobular liver injury, portal fibrosis, and HSC activation. F_2 rescued liver function and histopathological deterioration associated with CCl_4- and TAA-induced injury. F_2 effectively reduced the levels of fibrogenic markers (α-SMA, collagen I, PAI-1, and Fn1). Therefore, these results suggest that F_2 is a potential therapeutic agent to alleviate liver fibrosis in mice.

HSCs are a major source of myofibroblasts. Reports show that 82%–96% of myofibroblasts in CCl_4- and TAA-induced cholestatic and fatty liver disease are derived from HSCs [33]. HSCs can be activated by extrahepatic factors, cytokines, and cellular events in the injured liver microenvironment, among which TGF-β1 is prominent. Pathological TGF-β signaling leads to the activation of HSCs and the synthesis and deposition of ECM. TGF-β1 regulates the transcription of several fibrogenic genes via the canonical Smad-dependent pathway. Therefore, inhibiting TGF-β signaling and HSC activation may be a potential mechanism by which therapies for liver fibrosis could be developed. The human LX-2 HSC line was used in our experiments [34]. Our in vitro results showed that treatment of LX-2 cells with TGF-β1 led to HSC activation, while treatment with F_2 significantly reduced the production of ECM proteins (collagen I, PAI-1, FN1). F_2 also downregulated the expression of α-SMA, a myofibroblast marker, suggesting that F_2 could inhibit the activation of HSCs. In addition, F_2 suppressed fibrogenic gene expression by reducing the HSC response to TGF-β1 by reducing the expression of its receptor, TGFBR2, leading to a reduction in TGF-β/Smad signaling.

We further showed that F_2 not only reduced the levels of p-Smad2/3 and fibrogenic genes but also suppressed the expression of the TGF-β-binding receptor TGFBR2 in both activated HSCs and mouse models of liver fibrosis. Previous studies reported that the upregulation and activation of TGF-β1 and enhanced responses to TGF-β1 due to increased TGF-β receptor expression could enhance the activity of TGF-β1 during HSC activation [35]. Antagonizing

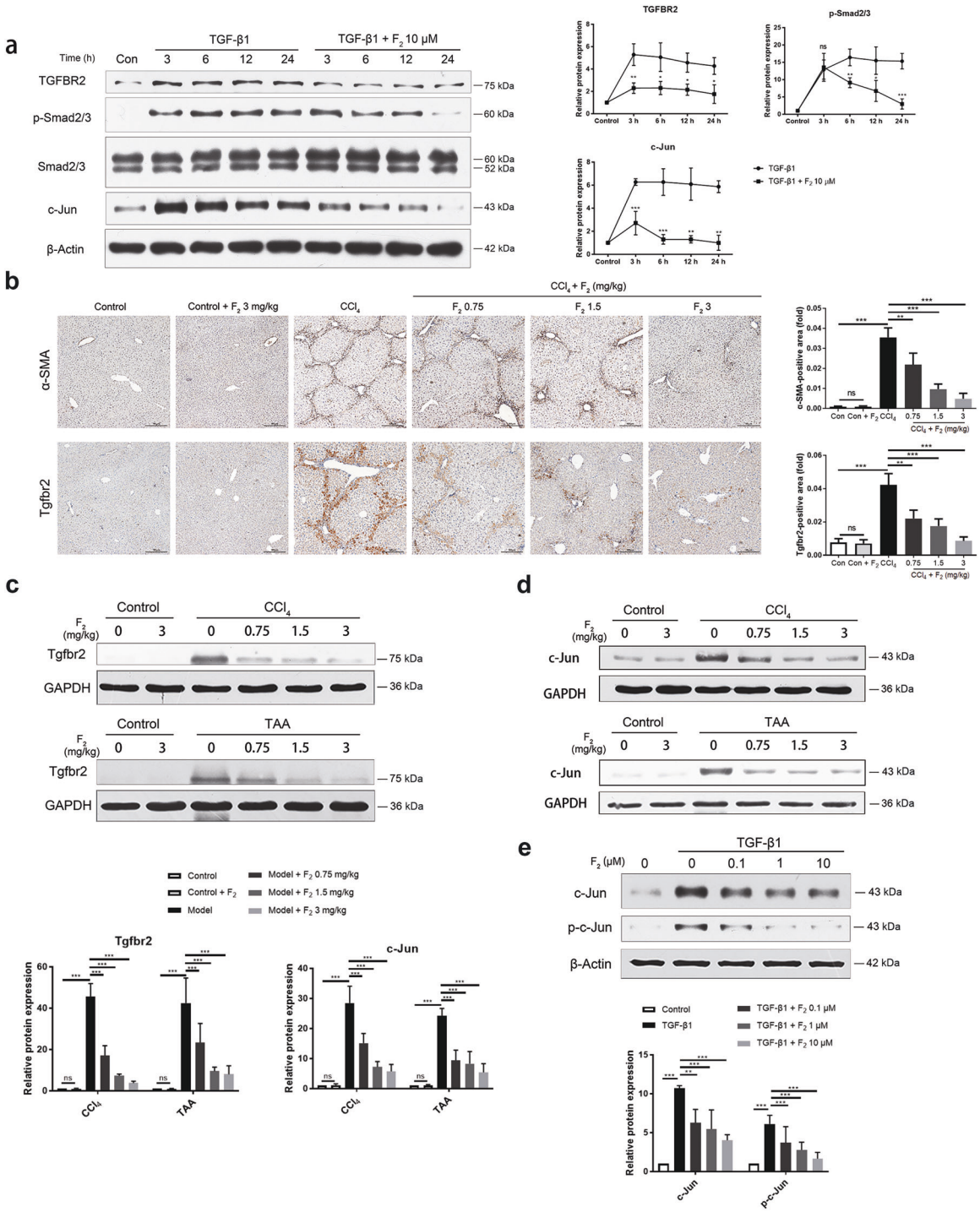

Fig. 4 F_2 decreases TGFBR2 and c-Jun expression in vivo and in vitro. **a** Effect of F_2 on the protein levels of TGFBR2, p-Smad2/3 and c-Jun at the indicated times in TGF-β1-induced LX-2 cells. $^*P < 0.05$; $^{**}P < 0.01$; $^{***}P < 0.001$ versus stimulation at the corresponding time points. **b** Representative images of immunohistochemical staining of α-SMA and Tgfbr2 (scale bar, 100 μm) in paraffin-embedded sections of liver tissues are shown, as well as densitometric quantification of the staining. **c**, **d** Protein expression levels of Tgfbr2 and c-Jun in liver samples from CCl_4- and TAA-induced fibrotic mice with or without F_2 treatment were analyzed by Western blotting. Quantitative analysis of Tgfbr2 and c-Jun expression in vivo. GAPDH expression was used as an internal reference. **e** Western blotting analysis of c-Jun and p-c-Jun protein expression in LX-2 cells. The values are the mean ± SD; $^*P < 0.05$; $^{**}P < 0.01$, $^{***}P < 0.001$, ns not significant, $n = 8$ mice per group in vivo, $n = 4$ cells per group in vitro.

TGF-β receptors and/or blocking their activation to inhibit TGF-β1 activity may be a major focus in the treatment of liver fibrosis [4]. Studies on pulmonary fibrosis have also shown that altering the expression of TGF-β receptors in lung injury can alter the cellular responses to TGF-β and promote fibrosis [36]. Downregulation or deletion of TGFBR2 in smooth muscle cells revealed the important role of this factor in the regulation of ECM genes [37, 38]. F_2 can downregulate TGFBR2 without significantly affecting TGFBR1 expression. This difference is probably due to differences in receptor trafficking and recycling [39].

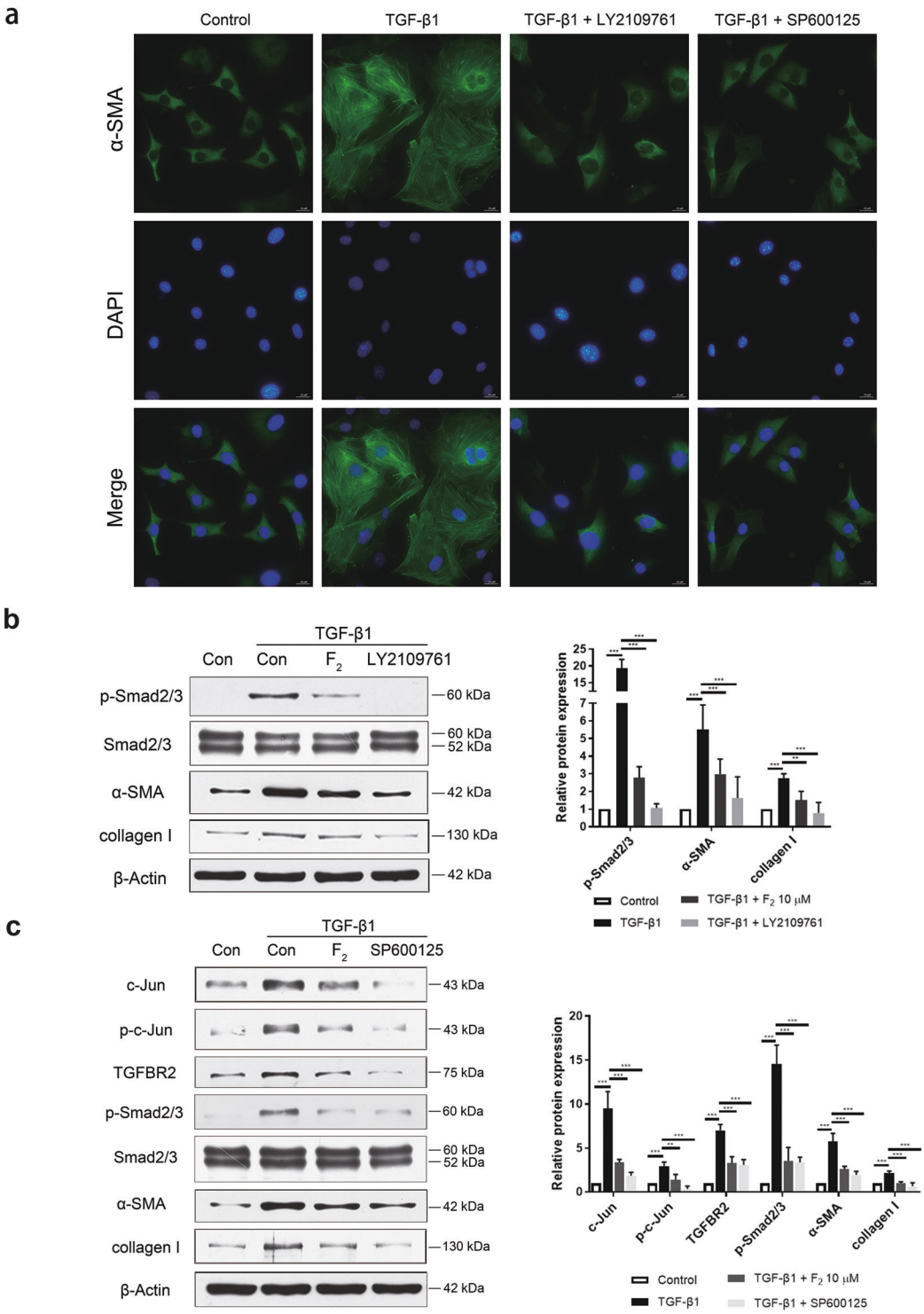

Fig. 5 Inhibiting c-Jun reduces TGF-β signaling. **a** Immunofluorescence staining of α-SMA (green, scale bar, 20 μm) in LX-2 cells. **b** Protein expression of p-Smad2/3, Smad2/3, α-SMA and collagen I was analyzed by Western blotting. **c** Protein expression of c-Jun, p-c-Jun, TGFBR2, p-Smad2/3, Smad2/3, α-SMA, and collagen I was analyzed by Western blotting. Quantitative analysis was performed using β-actin expression as the internal reference. The values are the mean ± SD; $^*P < 0.05$; $^{**}P < 0.01$; $^{***}P < 0.001$, ns not significant, $n = 4$ cells per group.

It has also been reported that several key transcription factors regulate the activation of HSCs. Transcription factors have a powerful regulatory role in the profibrogenic characteristics of activated HSCs [40]. AP-1 is a critical transcriptional regulator of HSC activation and is involved in numerous functions, including fibrogenesis, proliferation, α-SMA expression, and TIMP-1 production. Quiescent HSCs lack AP-1 expression but activation triggers the expression of Jun, Fos, and Fra [41]. c-Jun is a major component of AP-1. The transcription of c-Jun is rapidly stimulated by a number of extracellular signals, which activate the JNK or other MAP kinase pathways [42]. Previous studies indicate that nuclear c-Jun levels correlate with AP-1 target gene activity. Increased c-Jun levels may facilitate NASH development and progression [27]. Disease progression from steatosis to NASH

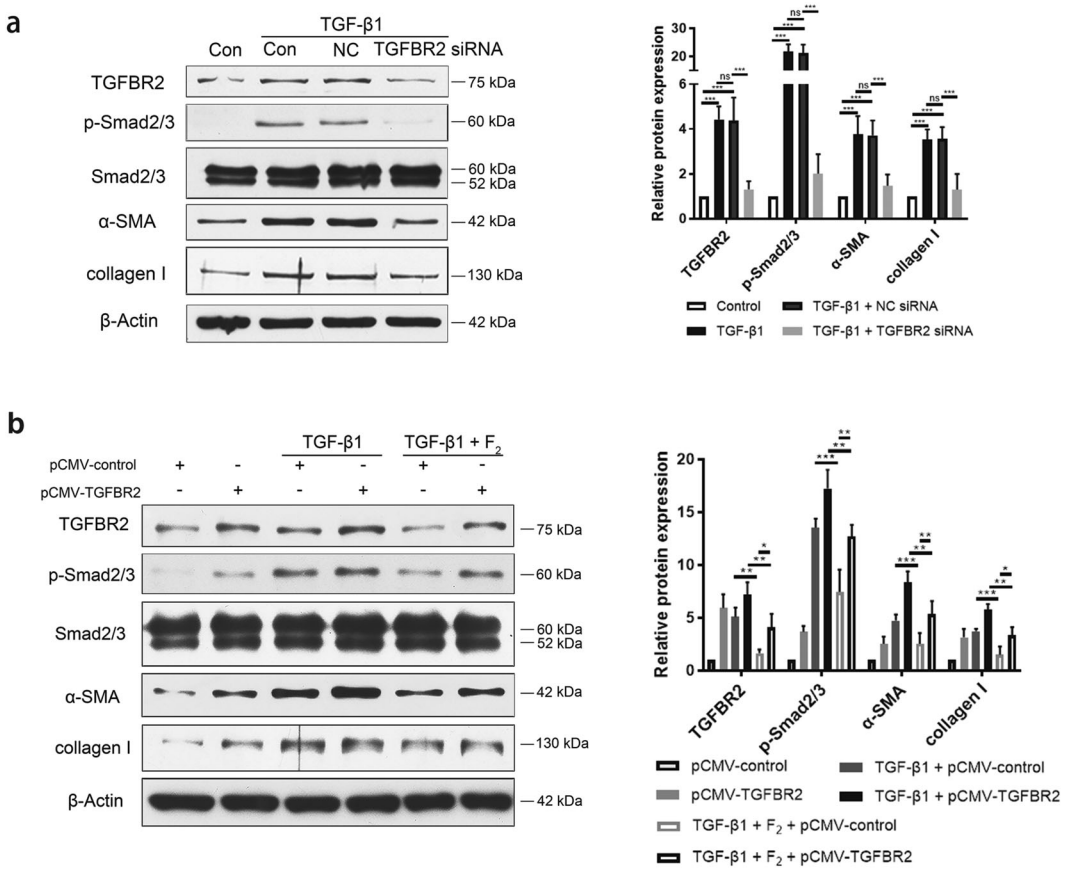

Fig. 6 Altering TGFBR2 expression influenced the antifibrotic effect of F_2. **a** TGFBR2 siRNA or negative control (NC) siRNA and **b** pCMV-TGFBR2 or pCMV-control were transfected into LX-2 cells. Twenty-four hours after transfection, the cells were subsequently induced with 5 ng/mL TGF-β1 with or without 10 μM F_2 for another 24 h. The protein expression of TGFBR2, p-Smad2/3, Smad2/3, α-SMA, and collagen I was analyzed by Western blotting and compared to that in the NC siRNA or vector group. Quantitative analysis was performed using β-actin expression as the internal reference. The values are the mean ± SD; $^*P < 0.05$; $^{**}P < 0.01$; $^{***}P < 0.001$, ns not significant, $n = 4$ cells per group.

in patients is associated with increased c-Jun expression, and in mice, c-Jun expression in nonparenchymal liver cells (NPLCs, including HSCs) promotes liver fibrosis [23]. c-Jun expression in NPLCs particularly correlated with fibrosis. It has been reported that decreases in c-Jun expression in HSCs reduce proliferation and α-SMA expression [43]. In this study, we showed that blocking c-Jun prevented the upregulation of TGFBR2 expression and fibrogenic gene levels in response to TGF-β1. As shown in Fig. 7a, immunofluorescence staining revealed the presence of c-Jun in the nucleus; c-Jun protein in whole cell lysates primarily reflects expression in the nuclear compartment. Considering the inhibitory effect of F_2 on c-Jun expression, it is possible that F_2 inhibits TGF-β signaling and fibrogenic gene expression by reducing c-Jun expression. This finding is consistent with a previous study by Fabre et al. that showed that blocking JNK phosphorylation inhibited the upregulation of TGFBR2 and p-Smad2/3 to prevent the induction of profibrotic genes in HSCs [44].

To further investigate the downregulation of TGFBR2 expression after F_2 administration, we focused on transcription because we found that F_2 also suppressed *TGFBR2* mRNA levels. We observed that F_2 decreased c-Jun expression, leading to decreased binding of c-Jun to the TGFBR2 promoter. Both c-Jun/AP-1 and SP-1 are known transcriptional regulators of TGFBR2 that directly activate TGFBR2 expression via promoter binding [28]. Bae et al. showed that the promoter region of the human TGFBR2 gene contains two positive regulatory elements (−219/−172, +1/+35), which have two potential recognition sequences for the transcription factors AP-1 and SP-1 [45]. This finding suggests that AP-1 and SP-1 play important regulatory roles in TGFBR2 expression. Our preliminary data showed that F_2 did not reduce the levels of SP-1, JunD, C-FOS, or ATF3 (Supplementary Fig. S5) but had an inhibitory effect on c-Jun expression. Our data further demonstrate that treatment with F_2 decreases the binding of c-Jun to the TGFBR2 promoter in a region where regulatory elements have been reported to enhance human TGFBR2 gene expression. Therefore, the reduction in c-Jun protein levels by F_2 influenced the activity of c-Jun to inhibit the binding of c-Jun to the TGFBR2 promoter. F_2 reduced TGFBR2 expression, following the decreased expression of c-Jun.

In our previous study on the cardiovascular system, we showed that F_2 protects against I/R- or H/R-induced myocardial injury by blocking membrane L-type Ca^{2+} channels [46]. Recently, we also showed that F_2 could protect cardiomyocytes through a calcium-independent pathway [10, 11] and protect cardiac microvascular endothelial cells, which have no L-type calcium channels [47]. Although some calcium channel blockers, such as verapamil and tetrandrine, have been reported to attenuate liver fibrosis, their antifibrotic effect is poor and may require large doses [48, 49]. To determine whether the antifibrotic effect of F_2 occurred through blocking calcium channels, we assessed the expression of α-SMA by Western blotting to compare the efficacies of 10 μM F_2, verapamil, and nifedipine. Only F_2 reduced the upregulation of α-SMA expression (Supplementary Fig. S6), suggesting that the mechanism by which F_2 protects against liver fibrosis may be independent of the calcium channel blocking effect at this dose. This study also showed that F_2 modulated c-Jun to alter the TGF-β1 response in HSCs, leading to a reduction in liver fibrosis.

In conclusion, F_2 inhibits fibrogenic gene expression in activated HSCs in vitro and ameliorates CCl_4- and TAA-induced

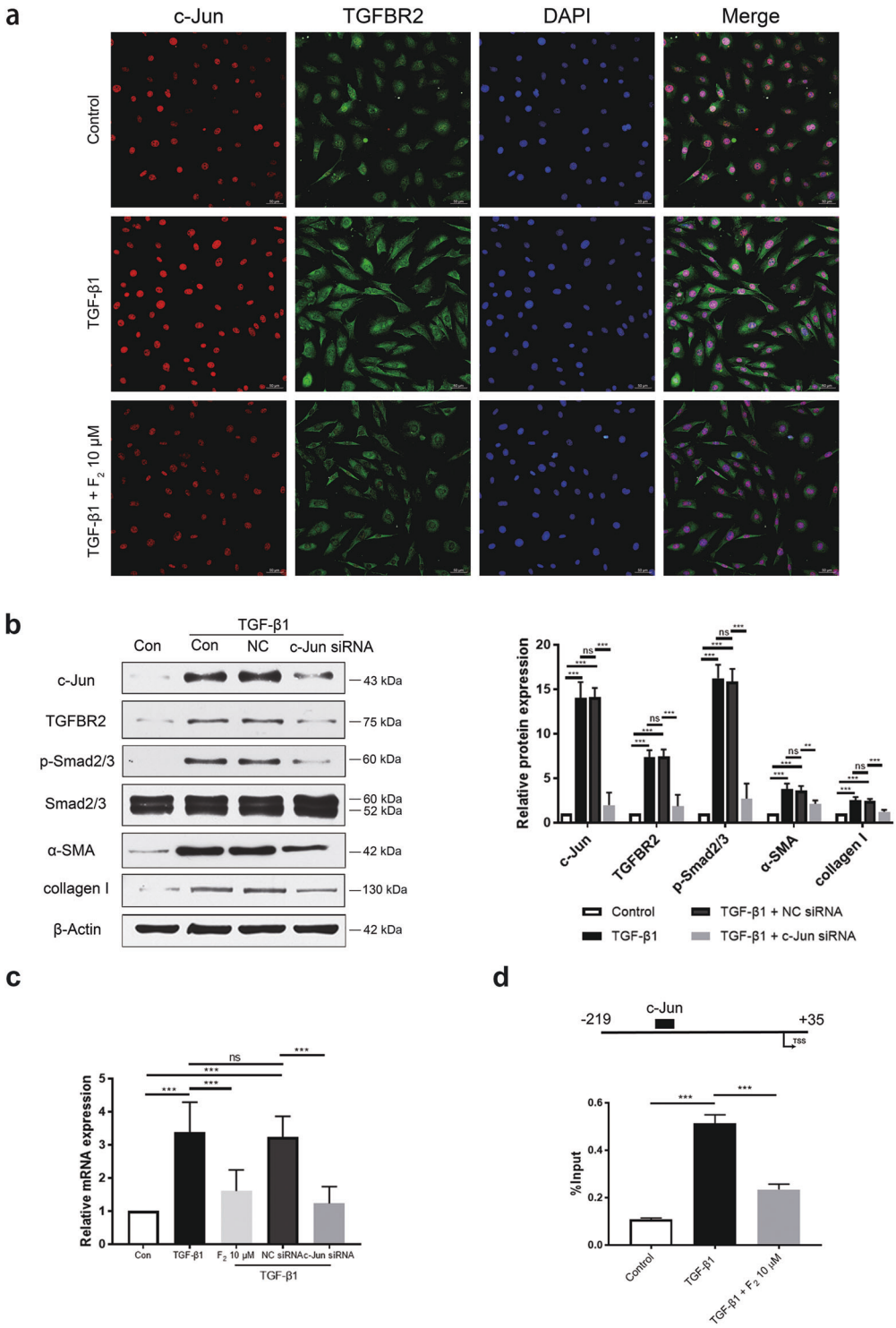

Fig. 7 c-Jun siRNA inhibits TGF-β signaling, and F_2 reduces the binding of c-Jun to the TGFBR2 promoter. a Immunofluorescence staining of c-Jun (red, scale bar, 50 μm) and TGFBR2 (green, scale bar, 50 μm) in LX-2 cells induced with 5 ng/mL TGF-β1 for 24 h with or without 10 μM F_2. **b** c-Jun siRNA reduced the protein levels of c-Jun, TGFBR2, p-Smad2/3, α-SMA, and collagen I in TGF-β1-induced LX-2 cells compared to those in the NC siRNA group, as assessed by Western blotting. Quantitative analysis was performed using β-actin expression as the internal reference. **c** The relative mRNA expression of *TGFBR2* was measured by RT-PCR. **d** A ChIP assay using an anti-c-Jun antibody was performed on TGF-β1-induced LX-2 cells treated with or without F_2. ChIP-DNA was analyzed by RT-PCR. The values are the mean ± SD; $^*P < 0.05$; $^{**}P < 0.01$; $^{***}P < 0.001$, ns not significant, $n = 4$ cells per group.

liver fibrosis in mice. F_2 exerts a beneficial effect by preventing c-Jun-induced TGFBR2 expression, thereby reducing the responsiveness of HSCs to TGF-β1 and concomitantly inhibiting activated HSCs (Fig. 8). This finding is consistent with current evidence showing that fibrosis is a dynamic process, and researchers should focus on pharmacotherapies to inhibit fibrogenesis in clinical settings. F_2 could be an effective antifibrotic agent.

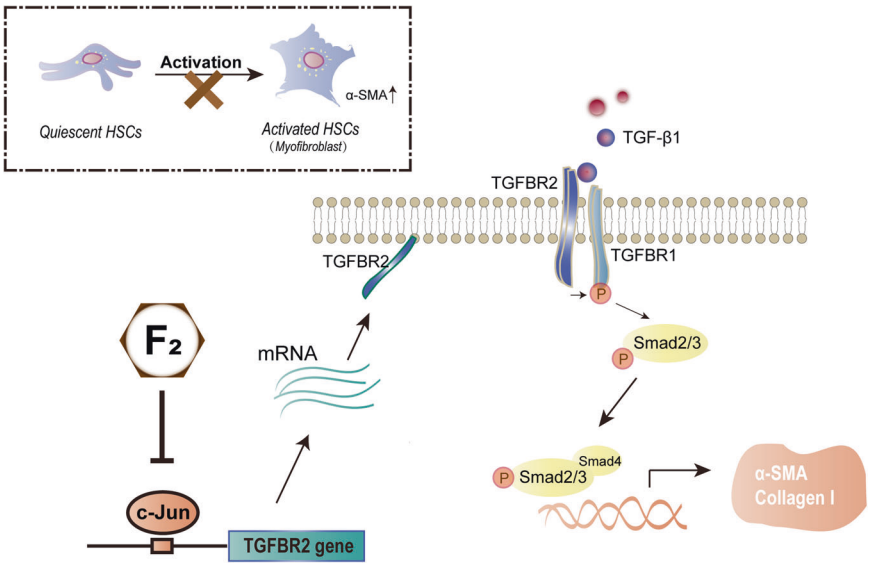

Fig. 8 Schematic diagram of the mechanism by which F_2 prevents liver fibrosis. F_2 inhibits hepatic stellate cell activation via the inhibition of c-Jun-induced TGFBR2 expression in the context of liver fibrosis.

ACKNOWLEDGEMENTS

This work was supported by the Research Team Project of the Natural Science Foundation of Guangdong Province of China (No. 9351503102000001). The authors thank the Pharmacological Department and Shantou University Medical College for providing the platform for our research.

AUTHOR CONTRIBUTIONS

GGS supervised the overall project, contributed reagents/materials/analysis tools, helped with the writing, and reviewed the paper. DFS performed the experiments and drafted the paper. GGS, DFS, and HC designed the experiments and analyzed the data. FFG, YMZ, and YDN provided technical guidance for the experiments and partly contributed reagents. WFC and BW aided in experimental critique, paper preparation, and figure preparation. BZC, QZ, and YBW provided support for the in vivo experiments, and ML and RJC provided support for the in vitro experiments.

ADDITIONAL INFORMATION

Supplementary information The online version contains supplementary material available at https://doi.org/10.1038/s41401-021-00630-7.

Competing interests: The authors declare no competing interests.

REFERENCES

1. Lee UE, Friedman SL. Mechanisms of hepatic fibrogenesis. Best Pract Res Clin Gastroenterol. 2011;25:195–206.
2. Bataller R, Brenner DA. Liver fibrosis. J Clin Invest. 2005;115:209–18.
3. Tsuchida T, Friedman SL. Mechanisms of hepatic stellate cell activation. Nat Rev Gastroenterol Hepatol. 2017;14:397–411.
4. Lee YA, Wallace MC, Friedman SL. Pathobiology of liver fibrosis: a translational success story. Gut. 2015;64:830–41.
5. Rotman Y, Sanyal AJ. Current and upcoming pharmacotherapy for non-alcoholic fatty liver disease. Gut. 2017;66:180–90.
6. Roehlen N, Crouchet E, Baumert TF. Liver fibrosis: mechanistic concepts and therapeutic perspectives. Cells. 2020;9:875.
7. Trautwein C, Friedman SL, Schuppan D, Pinzani M. Hepatic fibrosis: concept to treatment. J Hepatol. 2015;62:S15–24.
8. Huang ZQ, Shi GG, Zheng JH, Liu B. Effects of *N*-n-butyl haloperidol iodide on rat myocardial ischemia and reperfusion injury and L-type calcium current. Acta Pharmacol Sin. 2003;24:757–63.
9. Gao FF, Shi GG, Zheng JH, Liu B. Protective effects of *N*-n-butyl haloperidol iodide on myocardial ischemia-reperfusion injury in rabbits. Chin J Physiol. 2004;47:61–6.
10. Wang JZ, Cai CY, Zhang YM, Zheng JH, Chen YC, Li WQ, et al. *N*-n-Butyl haloperidol iodide protects against hypoxia/reoxygenation-induced cardiomyocyte injury by modulating protein kinase C activity. Biochem Pharmacol. 2010;79:1428–36.
11. Zhang Y, Chen G, Zhong S, Zheng F, Gao F, Chen Y, et al. *N*-n-butyl haloperidol iodide ameliorates cardiomyocytes hypoxia/reoxygenation injury by extracellular calcium-dependent and -independent mechanisms. Oxid Med Cell Longev. 2013; 2013:912310.
12. Zhang Y, Liao H, Zhong S, Gao F, Chen Y, Huang Z, et al. Effect of *N*-n-butyl haloperidol iodide on ROS/JNK/Egr-1 signaling in H9c2 cells after hypoxia/reoxygenation. Sci Rep. 2015;5:11809.
13. Lu S, Zhang Y, Zhong S, Gao F, Chen Y, Li W, et al. *N*-n-butyl haloperidol iodide protects against hypoxia/reoxygenation injury in cardiac microvascular endothelial cells by regulating the ROS/MAPK/Egr-1 Pathway. Front Pharmacol. 2016;7:520.
14. Huang ZQ, Jiang HY, Li JY, Liu XP, Zheng YS, Gao FF, et al. Effects of *N*-n-butly haloperidol iodide on the proliferation of intima and vascular muscle cells of rabbit carotid artery after balloon injury. Chin J Clin Pharmacol Ther. 2012;17:1112–7.
15. Rechtman MM, Nakaryakov A, Shapira KE, Ehrlich M, Henis YI. Different domains regulate homomeric and heteromeric complex formation among type I and type II transforming growth factor-beta receptors. J Biol Chem. 2009;284:7843–52.
16. Vaamonde-Garcia C, Malaise O, Charlier E, Deroyer C, Neuville S, Gillet P, et al. 15-Deoxy-Delta-12, 14-prostaglandin J2 acts cooperatively with prednisolone to reduce TGF-beta-induced pro-fibrotic pathways in human osteoarthritis fibroblasts. Biochem Pharmacol. 2019;165:66–78.
17. Fu X, Qie J, Fu Q, Chen J, Jin Y, Ding Z. miR-20a-5p/TGFBR2 axis affects pro-inflammatory macrophages and aggravates liver fibrosis. Front Oncol. 2020;10:107.
18. Fan W, Liu T, Chen W, Hammad S, Longerich T, Hausser I, et al. ECM1 prevents activation of transforming growth factor beta, hepatic stellate cells, and fibrogenesis in mice. Gastroenterology. 2019;157:1352–67.e13.
19. Shaulian E, Karin M. AP-1 as a regulator of cell life and death. Nat Cell Biol. 2002;4: E131–6.
20. Ryseck RP, Bravo R. c-JUN, JUN B, and JUN D differ in their binding affinities to AP-1 and CRE consensus sequences: effect of FOS proteins. Oncogene. 1991;6: 533–42.
21. Zhang Z, Gao Z, Hu W, Yin S, Wang C, Zang Y, et al. 3,3′-Diindolylmethane ameliorates experimental hepatic fibrosis via inhibiting miR-21 expression. Br J Pharmacol. 2013;170:649–60.
22. Trierweiler C, Hockenjos B, Zatloukal K, Thimme R, Blum HE, Wagner EF, et al. The transcription factor c-JUN/AP-1 promotes HBV-related liver tumorigenesis in mice. Cell Death Differ. 2016;23:576–82.
23. Schulien I, Hockenjos B, Schmitt-Graeff A, Perdekamp MG, Follo M, Thimme R, et al. The transcription factor c-Jun/AP-1 promotes liver fibrosis during non-alcoholic steatohepatitis by regulating osteopontin expression. Cell Death Differ. 2019;26:1688–99.
24. Seki E, Brenner DA, Karin M. A liver full of JNK: signaling in regulation of cell function and disease pathogenesis, and clinical approaches. Gastroenterology. 2012;143:307–20.
25. Kluwe J, Pradere JP, Gwak GY, Mencin A, De Minicis S, Osterreicher CH, et al. Modulation of hepatic fibrosis by c-Jun-N-terminal kinase inhibition. Gastroenterology. 2010;138:347–59.

26. Mederacke I, Dapito DH, Affo S, Uchinami H, Schwabe RF. High-yield and high-purity isolation of hepatic stellate cells from normal and fibrotic mouse livers. Nat Protoc. 2015;10:305–15.
27. Dorn C, Engelmann JC, Saugspier M, Koch A, Hartmann A, Muller M, et al. Increased expression of c-Jun in nonalcoholic fatty liver disease. Lab Invest. 2014;94:394–408.
28. Song K, Wang H, Krebs TL, Kim SJ, Danielpour D. Androgenic control of transforming growth factor-beta signaling in prostate epithelial cells through transcriptional suppression of transforming growth factor-beta receptor II. Cancer Res. 2008;68:8173–82.
29. Chen A. Acetaldehyde stimulates the activation of latent transforming growth factor-beta1 and induces expression of the type II receptor of the cytokine in rat cultured hepatic stellate cells. Biochem J. 2002;368:683–93.
30. Weber LW, Boll M, Stampfl A. Hepatotoxicity and mechanism of action of haloalkanes: carbon tetrachloride as a toxicological model. Crit Rev Toxicol. 2003;33:105–36.
31. Wallace MC, Hamesch K, Lunova M, Kim Y, Weiskirchen R, Strnad P, et al. Standard operating procedures in experimental liver research: thioacetamide model in mice and rats. Lab Anim. 2015;49:21–9.
32. Strnad P, Tao GZ, Zhou Q, Harada M, Toivola DM, Brunt EM, et al. Keratin mutation predisposes to mouse liver fibrosis and unmasks differential effects of the carbon tetrachloride and thioacetamide models. Gastroenterology. 2008;134:1169–79.
33. Mederacke I, Hsu CC, Troeger JS, Huebener P, Mu X, Dapito DH, et al. Fate tracing reveals hepatic stellate cells as dominant contributors to liver fibrosis independent of its aetiology. Nat Commun. 2013;4:2823.
34. Xu L, Hui AY, Albanis E, Arthur MJ, O'Byrne SM, Blaner WS, et al. Human hepatic stellate cell lines, LX-1 and LX-2: new tools for analysis of hepatic fibrosis. Gut. 2005;54:142–51.
35. Kim Y, Ratziu V, Choi SG, Lalazar A, Theiss G, Dang Q, et al. Transcriptional activation of transforming growth factor beta1 and its receptors by the Kruppel-like factor Zf9/core promoter-binding protein and Sp1. Potential mechanisms for autocrine fibrogenesis in response to injury. J Biol Chem. 1998;273:33750–8.
36. Zhao Y, Shah DU. Expression of transforming growth factor-beta type I and type II receptors is altered in rat lungs undergoing bleomycin-induced pulmonary fibrosis. Exp Mol Pathol. 2000;69:67–78.
37. Zhao N, Koenig SN, Trask AJ, Lin CH, Hans CP, Garg V, et al. MicroRNA miR145 regulates TGFBR2 expression and matrix synthesis in vascular smooth muscle cells. Circ Res. 2015;116:23–34.
38. Jaffe M, Sesti C, Washington IM, Du L, Dronadula N, Chin MT, et al. Transforming growth factor-beta signaling in myogenic cells regulates vascular morphogenesis, differentiation, and matrix synthesis. Arterioscler Thromb Vasc Biol. 2012;32:e1–11.
39. Akhurst RJ, Padgett RW. Matters of context guide future research in TGFbeta superfamily signaling. Sci Signal. 2015;8:re10.
40. Mann J, Mann DA. Transcriptional regulation of hepatic stellate cells. Adv Drug Deliv Rev. 2009;61:497–512.
41. Mann DA, Smart DE. Transcriptional regulation of hepatic stellate cell activation. Gut. 2002;50:891–6.
42. Mathas S, Hinz M, Anagnostopoulos I, Krappmann D, Lietz A, Jundt F, et al. Aberrantly expressed c-Jun and JunB are a hallmark of Hodgkin lymphoma cells, stimulate proliferation and synergize with NF-kappa B. EMBO J. 2002;21:4104–13.
43. Liu XJ, Yang L, Mao YQ, Wang Q, Huang MH, Wang YP, et al. Effects of the tyrosine protein kinase inhibitor genistein on the proliferation, activation of cultured rat hepatic stellate cells. World J Gastroenterol. 2002;8:739–45.
44. Fabre T, Kared H, Friedman SL, Shoukry NH. IL-17A enhances the expression of profibrotic genes through upregulation of the TGF-beta receptor on hepatic stellate cells in a JNK-dependent manner. J Immunol. 2014;193:3925–33.
45. Bae HW, Geiser AG, Kim DH, Chung MT, Burmester JK, Sporn MB, et al. Characterization of the promoter region of the human transforming growth factor-beta type II receptor gene. J Biol Chem. 1995;270:29460–8.
46. Huang Y, Gao F, Zhang Y, Chen Y, Wang B, Zheng Y, et al. *N*-n-Butyl haloperidol iodide inhibits the augmented Na^+/Ca^{2+} exchanger currents and L-type Ca^{2+} current induced by hypoxia/reoxygenation or H_2O_2 in cardiomyocytes. Biochem Biophys Res Commun. 2012;421:86–90.
47. Zhou Y, Zhang Y, Gao F, Guo F, Wang J, Cai W, et al. *N*-n-butyl haloperidol iodide protects cardiac microvascular endothelial cells from hypoxia/reoxygenation injury by down-regulating Egr-1 expression. Cell Physiol Biochem. 2010;26:839–48.
48. Xu D, Wu Y, Liao ZX, Wang H. Protective effect of verapamil on multiple hepatotoxic factors-induced liver fibrosis in rats. Pharmacol Res. 2007;55:280–6.
49. Hsu YC, Chiu YT, Cheng CC, Wu CF, Lin YL, Huang YT. Antifibrotic effects of tetrandrine on hepatic stellate cells and rats with liver fibrosis. J Gastroenterol Hepatol. 2007;22:99–111.